Journal of Applied Electrochemistry (2007) 37:147–153
DOI 10.1007/s10800-006-9226-8

Platinum supported on resorcinol–formaldehyde based carbon aerogels for PEMFC electrodes: Influence of the carbon support on electrocatalytic properties

JULIEN MARIE[1,*], SANDRINE BERTHON-FABRY[1], MARIAN CHATENET[2], ERIC CHAINET[2]
RENÉ PIRARD[3], NATHALIE CORNET[4] and PATRICK ACHARD[1]
[1]*CEP ENSMP, BP 207 06904, Sophia Antipolis Cedex, France*
[2]*LEPMI-ENSEEG, UMR 5631 CNRS-INPG-UJF, BP 75 38402, Saint Martin d'Hères Cedex, France*
[3]*Laboratoire de Génie Chimique, University of Liège, B-4000, Liège, Belgium*
[4]*RENAULT, TCR- DR/64240, 78288, Guyancourt, France*
*(*author for correspondence, tel.: + 33-493-957-495; fax: + 33-493-957-535; e-mail: julien.marie@ensmp.fr)*

Received 14 February 2006; accepted in revised form 15 August 2006

Key words: carbon aerogels, PEMFC cathode, platinum

Abstract

Two carbon aerogels with different nanopore size distributions but both with high surface area, high nanoporous volume and low bulk density have been compared as platinum support. The influence of the nanostructure of the carbon aerogel on the platinum nanoparticle deposit was investigated. The platinum was deposited on the carbon by means of two different techniques, one employing an anionic platinum precursor, the other using a cationic one. The porosity of the carbon aerogels was characterized by combining N_2-sorption and mercury porosimetry. The platinum deposit was characterized by transmission electron microscopy and rotating disk electrode experimentation to measure the platinum active surface area and its activity towards oxygen reduction reaction (ORR). The structural differences between the carbon aerogels did not yield any difference in platinum deposits in terms of Pt-surface area and ORR activity. Interestingly, the ORR mass activity of the high Pt-surface area samples, obtained by the cationic insertion technique, was several times lower than that of the samples obtained by the anionic technique. This observation was attributed to the particle size effect, detrimental in the case of platinum particle size around 1 nm.

1. Introduction

The hydrogen/air-fed polymer electrolyte membrane fuel cell (PEMFC) is an attractive power source because of its high power density [1], high efficiency [2] and cleanliness. The continual improvement of its performance during the past decades [3] is a chance to turn to a cleaner automotive society [4, 5]. Nevertheless, before a PEMFC can compete with an internal combustion engine, its price must be reduced. Therefore the quantity of costly platinum used in PEMFC electrodes as electrocatalyst must be reduced; all the more since it is a limited natural resource [6]. One way of achieving platinum quantity reduction without reducing cell performance is to find new cathode catalytic layer structures to reduce the gas diffusion limitations at the air-fed cathode [7]. Up to now, PEMFC catalytic layers described in the literature are usually structured by a carbon black used as the catalyst support [8]. Even though a wide range of different carbon blacks exists, their replacement by a carbon aerogel should lead to significant changes in the catalytic layer structure. Indeed, carbon aerogels have monolithic porous structure whereas carbon blacks are aggregates. In other words, the arrangement of the spherical carbon nanoparticles which they are both made of, called primary carbon nanoparticles, differ greatly. The primary carbon nanoparticles of a carbon black are fused together in clusters of a few tens of particles covalently linked and called aggregates. Such aggregates are usually agglomerated through Van der Waals stabilizing interactions. In the case of carbon aerogels, the primary carbon nanoparticles are tridimensionally linked through covalent bonds to form a macroscopic monolithic structure with high porosity (more than 90% of void space) with good electronic conductivity (>1 S cm^{-1}) [9]. This particular structure of the carbon aerogels prevents the formation of small or even closed pores (inside aggregates) [10] in the catalytic layer of the PEMFC and their large mesoporosity should enable better proton conducting ionomer penetration into the layer while keeping part of the pores unfilled for the access of reactant gas. Hence, the RF-based carbon aerogels synthesized in this study are promising electrocatalyst supports of the PEMFC cathode because of their high surface area, high nanoporous volume, and adjustable

pore-size distribution. Carbon aerogels have already been used in PEMFC electrodes [11] but the influence of the carbon aerogel pore-size distribution on the platinum electrocatalyst properties has not yet been studied. Regarding carbon blacks, it has been shown that changing the type of carbon black yields important differences in the platinum deposit properties [12, 13]. In addition, carbon aerogels, first developed in 1989 by Pekala [14], are a relatively new type of porous carbon material so it is worth raising the question of the influence of the carbon aerogel structure on the properties of the platinum deposit for future optimization of PEMFC cathode catalytic layers. Two different carbon aerogels have been synthesized for this purpose and the platinum deposits obtained with two different techniques are compared on each carbon so that conclusions about the influence of the nanostructure of the carbon aerogel on the platinum deposit are not limited to a single kind of deposit.

2. Experimental

2.1. *Carbon aerogel synthesis*

The carbon aerogels CA#1 and CA#2 were synthesized from resorcinol (R)-formaldehyde (F) sol with F/R = 2 molar ratio dissoluted into distilled and deionized water. The gelation catalyst (C) was sodium carbonate. The sol underwent gelation in sealed glass tubes at 80 °C for 3 days. The reactant molar ratios (R/C) are presented in Table 1, as well as the mass fraction of reactants in the sol (%solid) defined as $\%\text{solid} = (m_R + m_F + m_C)/V_{H_2O}$.

The obtained gels were dried under supercritical conditions of CO_2. The water filling the pores of the gels was previously exchanged with acetone. The dry organic aerogels were pyrolyzed at 1050 °C for 30 min under flowing nitrogen (3 l min^{-1}).

Table 1. Results of the morphology characterization of two carbon aerogels CA#1 and CA#2 with different sol–gel synthesis parameters R/C and %solid: bulk-density ρ_b, BET surface area S_{BET}, microporous volume V_{mic}, mesoporous volume V_{mes}, mercury porosimetry cumulated volume V_{Hg}, and void volume V_V

Sample	CA#1	CA#2
R/C	300	200
%solid	5	10
ρ_b/g cm^{-3} ± 5%	0.15	0.19
$S_{BET}/m^2\ g^{-1}$ ± 5%	669	565
V_{mes}*/$cm^3\ g^{-1}$ ± 5%	0.55–0.8	0.66–1.6
V_{mes}(2–7.5)**/$cm^3\ g^{-1}$ ± 5%	0.12	0.09
$V_{mic}/cm^3\ g^{-1}$ ± 5%	0.33	0.26
$V_{Hg}/cm^3\ g^{-1}$ ± 5%	5.15	4.45
$V_p/cm^3\ g^{-1}$ ± 5%	5.6	4.8
$V_V/cm^3\ g^{-1}$ ± 10%	6.1	4.73

*Full mesoporous porous volume measured from N_2-sorption: 2–50 nm

**Part of the mesoporous porous volume measured from N_2-sorption between 2 and 7.5 nm

2.2. *Platinum insertion onto carbon aerogel*

2.2.1. *Pt-insertion on raw carbon aerogel*

Finely grinded carbon aerogel powder samples were suspended in a H_2PtCl_6 water solution with a platinum concentration of 1.2 g l^{-1} and a mass ratio Pt/(Pt + C) equal to 0.4. The pH of this impregnation solution was 2.2 ± 0.1 which was expected because the platinum salt is a strong acid. After 24 h of magnetic stirring, the reducing agent $NaBH_4$ was added to the suspension as an aqueous solution (0.1 M). The amount of $NaBH_4$ added was 8 times the stoichiometric quantity of Pt to ensure complete reduction of the platinum salt. The Pt-doped carbon aerogel powder was then washed thoroughly with boiling water and filtered before being dried.

2.2.2. *Platinum insertion onto oxidized carbon aerogel*

The carbon aerogel surface oxidation was necessary for the platinum insertion to occur when using the cationic platinum precursor $Pt(NH_3)_4(OH)_2$ [15, 16]. The oxidizing treatment was done as follows. The carbon aerogels powder samples were suspended (10 g l^{-1}) in 4 M HNO_3 at 80 °C for 24 h. The oxidized carbon aerogels (oxCA) were then thoroughly washed with water and filtered. The resulting carbon aerogel powder was then suspended in a $Pt(NH_3)_4(OH)_2$ solution. The platinum and carbon concentrations were 4.7 and 4 g l^{-1}, respectively. The pH of the impregnation solution remained constant (11 ± 0.1) after a few minutes of magnetic stirring until the end of the 24 h impregnation. The powder was then filtered and dried in air at 90 °C before being placed in a tubular quartz oven for the reduction. The platinum salt adsorbed on the carbon surface was first decomposed under a nitrogen flow rate of 10 $cm^3\ min^{-1}$ at 350 °C for 1 h and then reduced by changing nitrogen to hydrogen.

2.3. *Material characterization*

2.3.1. *Carbon aerogel morphology analysis*

The carbon aerogel structure was characterized from nitrogen sorption isotherm analysis at 77 K on a Carlo Erba Sorptomatic 1900 device. The surface area (S_{BET}), microporous volume (V_{mic}) and mesoporous volume (V_{mes}) was calculated using the Brunauer, Emmet and Teller (BET) method [17], the Dubinin–Radushkevitch method [18] and the Broekhoff-de-Boer (BdB) model on the desorption isotherm with a form factor of 2 (cylindrical pores) [19] respectively, as appropriate. The measurement of the bulk density of the carbon aerogel monoliths by mercury pycnometry served to calculate the "void" volume (V_V) of the monoliths from the following formula:

$$V_V = 1/\rho_b - 1/\rho_s \quad (1)$$

with ρ_s the skeleton density taken equal to 2.1 ± 0.1 g cm^{-3} which is a common value obtained by helium pycnometry on RF-based carbon aerogels [20].

In addition, the porous volume of the carbon aerogels was measured by mercury porosimetry on a Carlo Erba Porosimeter 2000 (2000 bar maximum pressure). The Hg-porosimeter was used at its lowest pressure sweep rate so that the porous volume data was recorded at equilibrium. This enabled the porous volume corresponding to pore-size larger than 7.5 nm (V_{Hg}) to be obtained. Thus, the total porous volume (V_p) was obtained by adding several measured volumes as follows:

$$V_p = V_{mic} + V_{mes(2-7.5nm)} + V_{Hg} \quad (2)$$

where $V_{mes(2\text{-}7.5nm)}$ represents the 2–7.5 nm pore-size fraction of the mesoporous volume measured from N_2-sorption. The experimental data (Table 1) show that the mercury porous volume V_{Hg} represents the major part of the porous volume V_p. The value of V_p compares well with that of V_V, particularly for CA#2. Considering the possible large error on mercury pycnometry, V_P can be considered as very reliable with only ± 5% measurement error.

2.3.2. *Platinum deposit characterization*

The platinum and carbon atomic fractions in the samples were measured by elemental analysis with a flame atomic absorption spectrometer after dissolving the platinum supported on the carbon aerogel surface in aqua regia. The platinum deposit structure was observed by means of a transmission electron microscope (TEM). The electrochemical characterization was made on a rotating disk electrode (RDE) with a 0.196 cm^2 glassy carbon surface area (EDT 101, Tacussel) in a three-electrode cell controlled by a potentiostat PAR 273 (EG&G) with a saturated calomel electrode (SCE) as reference (+0.241 V vs NHE). Measurements were carried out on a thin layer of Pt-supported carbon aerogel (Pt/CA). The layer was made by depositing on the EDT a 10 μl drop of an ink (sonicated for 1 h) comprising 10^{-3} g of Pt/CA, 0.2 g of a 10 wt%-Nafion solution in water (Ion Power Inc.) and 1 g of 18.2 MΩ cm water (MilliQ element). The platinum surface loadings of the layers were between 40 and 80 $\mu g\ cm^{-2}$ depending on the different platinum mass-fractions of the samples but the amount of carbon was the same for all the measurements (215 ± 10 $\mu g\ cm^{-2}$). Such platinum loadings are higher than those employed in the so-called thin-film RDE technique [7]. Such a relatively large amount of Pt/CA is used on the EDT in order to increase the absolute measured signal amplitude (intensity) i.e. to lower the measurement error. The platinum surface area was measured from hydrogen-adsorption/desorption coulometry. For this technique, the cell was first inerted by N_2 bubbling in the solution for 15 min and while keeping the inert gas stream above the solution, 10 voltammetric cycles at 0.1 V s^{-1} between hydrogen evolution potential (0 V vs NHE) and 1.441 V vs NHE were applied. The active area of platinum was determined from the coulometric charge under the hydrogen-desorption peaks in the last cycle, using the value 220 × 10^{-6} C cm^{-2} of platinum. In order to measure the activity of the catalysts, oxygen reduction reaction (ORR) voltammetry was performed. During the experiment, the O_2 concentration in the cell was kept at its saturation value by gentle O_2-bubbling. The quasi-steady-state voltammograms were recorded at 10^{-3} V s^{-1} from 0.941 to 0.141 V vs NHE. The experiments were repeated at 3 RDE rotation speeds (52, 104 , 209 rad s^{-1}) and the average intensity was used in the calculations. The kinetic current density was calculated from the well known formula:

$$i_k = \frac{i.i_l}{i_l - i} \quad (3)$$

where i_l is the limiting current as described by Bard and Faulkner [21].

The Tafel slopes of the ORR reaction on Pt/CA were drawn by fitting the Tafel plots of the kinetic current density measurements between 0.95 and 0.85 V vs NHE. In order to compare the catalytic activities of the different samples, the kinetic current density measured at 0.841 V vs NHE corresponding to 0.39 V ORR overpotential in 1 M sulphuric acid which is a practical PEMFC overpotential are given normalized to either the platinum active area or the mass of platinum.

3. Results

3.1. *Morphology of the carbon aerogels*

The sorption isotherms of CA#1 and CA#2 carbon aerogels shown on Figure 1 can hardly be classified as one of the six particular types of sorption isotherms of the IUPAC classification [22]. Indeed, the contributions to the adsorbed volume of different ranges of pore-sizes (namely mesopores and macropores) seem to be observed on the sorption isotherms. The existence of mesopores would be indicated by hysteresis between adsorption and desorption isotherms which is usually associated with type IV isotherms

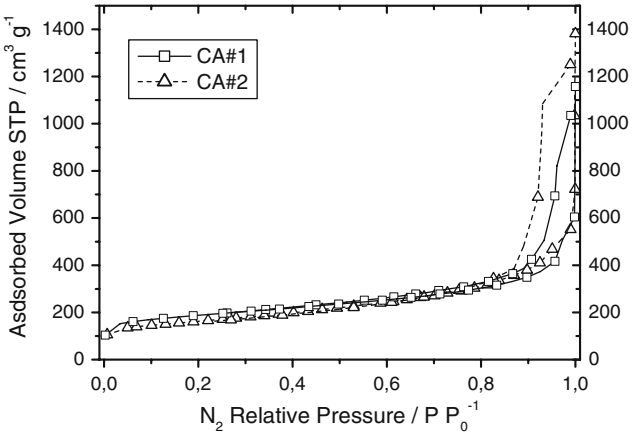

Fig. 1. Nitrogen adsorption isotherms for the two carbon aerogels CA#1 & 2.

but this type of isotherm is also characterized by a slanted plateau-like region near the saturation ($P/P_0 \approx 1$), which cannot be seen in Figure 1. Isotherms tangential to the P/P_0-axis are characteristic of type II isotherms indicating the presence of macropores. Therefore Figure 1 isotherms may be presented as type II with a hysteresis loop indicating the presence of both mesopores and macropores in CA#1 and CA#2 carbon aerogels.

The morphological properties of the two carbon aerogels are gathered in Table 1. The amount of micropores (V_{mic}) computed by the Dubinin–Radushkevitch equation is validated by the value of the radius of the micropores obtained from the energy of the interaction given by the slope of the regression which is 0.77 nm, well in the microporous range.

Carbon aerogel CA#1 has a higher BET surface area than the CA#2 which is at first surprising because it is constituted of larger primary carbon particles (10 nm diameter for CA#1 vs 6 nm for CA#2) as shown in Figure 3. But this apparent contradiction no longer exists when comparing the two microporous volumes. Indeed, CA#1 has a higher microporous volume (and thus more micropores) which yields higher surface area (micropores contribute much more to the total surface area than to the total porous volume). This means that larger primary RF-aerogel particle allows for the formation of a larger number of micropores during the pyrolysis.

As shown in Table 1, V_{mes} is far below V_p or V_V for both carbon aerogels which is an indication of the existence of macropores. The contribution of macropores to the porous volume cannot be quantified because of the asymptotic shape of the isotherm near the saturation. This asymptotic shape is also the reason why two values of V_{mes} are given in Table 1, one calculated from the adsorption isotherm (smaller value) and the other calculated from the desorption isotherm. Another explanation for the low mesopore volume is the possible cessation of capillary condensation (i.e. the nitrogen meniscus negative curvature disappears) in large mesopores before complete filling. This occurs because of the typical structure of aerogels which are made of interconnected filament-like aggregates in which the curvature of the adsorbed nitrogen meniscus goes to zero before complete filling [23]. This entails unmeasured porous volume even though the pores are smaller than 50 nm. It appears that CA#1 and CA#2 illustrate two different cases. Indeed, the pore size distribution calculated by the BdB method (similar to BJH) shown on Figure 2 reveals that CA#2 has the largest part of its porous volume (4.8 $cm^3\ g^{-1}$) made up of pores in the mesoporous range (34 ± 4 nm) but the value of the mesoporous volume V_{mes} is underestimated because the nitrogen capillary condensation ceases before complete filling of the aerogel mesopores. In the case of CA#1, no significant contribution to the porous volume is found in the mesopore range which should

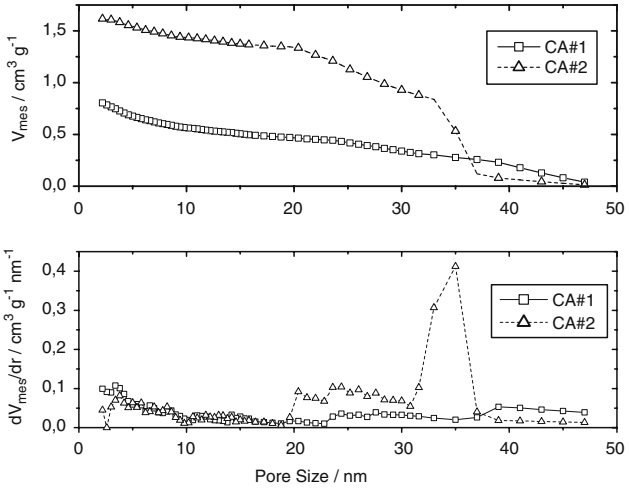

Fig. 2. Broekhoff-de-Boer cumulated porous volume (top) and pore-size distribution (bottom) as a function of the pore size (r) for two carbon aerogels CA#1 & 2 calculated from the desorption isotherms with a form factor of 2 (cylindrical pores).

mean that the full porous volume of CA#1 (5.6 $cm^3\ g^{-1}$) is essentially constituted of pores larger than 50 nm.

In support of these considerations (all based on modelling), TEM observations were carried out. The 2D-projection (inherent to the TEM technique) of the 3D-structure of the void spaces between the primary carbon particles can give an estimation of the size of the pores and is a useful way of comparing the carbon aerogel structures as shown in Figure 3. The observed pore-sizes on the pictures are 25–66 nm for CA#1 and 15–40 nm for CA#2 which is, for CA#2, in good agreement with the BdB pore-size range (34 ± 4 nm). As for CA#1, its porous volume would be essentially constituted of pores in the 50–66 nm range.

3.2. *Platinum deposit characterization*

The comparison of the platinum loadings (Table 2) reveals that platinum insertion on oxidized carbon aerogel does not yield as high loading as insertion on raw carbon. In the case of the insertion of H_2PtCl_6, almost all of the platinum initially introduced in the impregnation solution (40 wt%) has been fixed on the carbon. The insertion of the cationic platinum precursor $Pt(NH_3)_4(OH)_2$ is governed by its ion-exchange with the protons of the carbon surface oxides rather than physisorption on the carbon surface as in the case of H_2PtCl_6 impregnation on the raw carbon aerogels. So increasing the platinum content of Pt/oxCA would have been possible by exposing the carbon aerogel to a stronger oxidising treatment (e.g. increase in temperature or acid concentration) but this would have probably changed the structure of the carbon [24] (i.e. giving oxCA and CA different structures) and the comparison of the two carbon aerogel structures CA#1 and CA#2 supported by two different insertion techniques would not have been relevant.

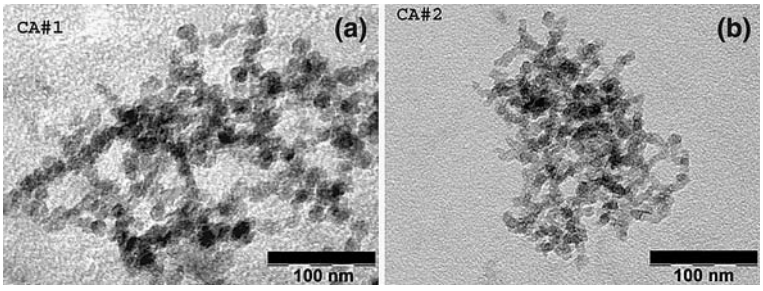

Fig. 3. TEM pictures showing the voids between the primary carbon particles of carbon aerogels (a) CA#1 and (b) CA#2.

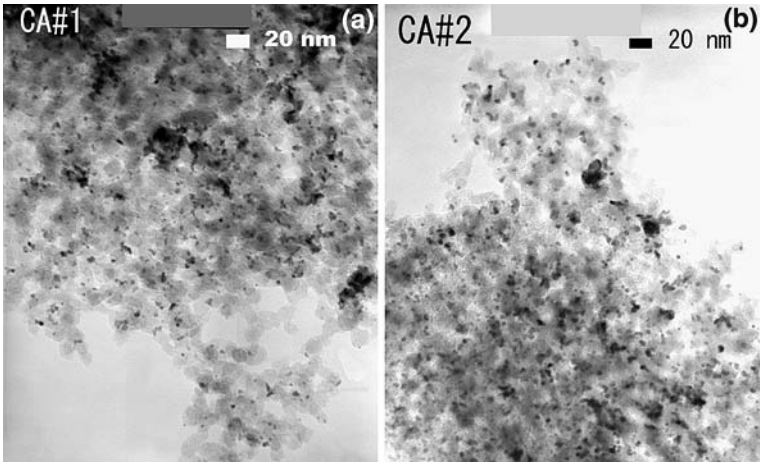

Fig. 4. TEM pictures showing platinum nanoparticles (black) deposited on raw carbon aerogel (grey) (a) CA#1 and (b) CA#2.

3.2.1. *Transmission electron microscope observation*

The platinum nanoparticle dispersion on raw carbon aerogel (Figure 4) is similar on CA#1 and CA#2. The platinum nanoparticle average size is 4 ± 1 nm. A large majority of the platinum particles are well distributed on the carbon aerogel surface. Nevertheless, some have agglomerated and form 10 nm black areas on the picture (the resolution is not sufficient to distinguish particles inside the aggregates).

Concerning the platinum dispersion on the oxidized carbon aerogels (Figure 5), it is very difficult to distinguish platinum from carbon since the platinum particles are very small. There is almost no contrast between very small black platinum particles and the carbon aerogel surface. The platinum particle size is estimated to be smaller than 1.5 nm (on CA#1 and CA#2) and no agglomeration was observed.

3.2.2. *Electrochemical characterization*

The voltammograms shown in Figure 6 reveal hydrogen desorption on platinum peaks separated from the carbon signal background by the horizontal line in the zone (−0.25 to 0.15 V vs SCE). The coulometry of these peaks yields the platinum active area as explained in [25]. The CA#1 and CA#2 signals cannot be differentiated either in the case of Pt/CA samples or the Pt/oxCA samples. The platinum surface areas are the same on CA#1 and CA#2 as reported in Table 2. This confirms the TEM observation which showed platinum deposit on CA#1 and CA#2 with similar structures.

The voltammograms of Pt/oxCA (Figure 6) samples bring to light a commonly observed feature on oxidized carbon surfaces [26], namely quinone/hydroquinone oxido-reduction currents in the 0.2–0.6 V. vs SCE range (wide peak indicated by the arrows).

Table 2. Electrochemical characterization of Pt deposit on raw carbon aerogels and oxidized carbon aerogels: specific surface area S_{Pt}, specific intensity i_{spec} and surface intensity i_{surf} measured at 0.841 V/NHE, Tafel slope

Samples	Pt/CA#1	Pt/CA#2	Pt/oxCA#1	Pt/oxCA#2
Pt loading/wt% Pt ± 2%	31.1	30.4	14.9	13.8
Carbon Loading/wt% C ± 2%	58	57	70	72
$S_{Pt}/m^2\ g_{Pt}^{-1}$ ± 5%	43	44	115	125
i_m @ 0.841 V vs NHE/A g_{Pt}^{-1} ± 5%	28	29	9	11
i_{surf} @ 0.841 V vs NHE/μA $cm^{-2}{}_{Pt}$ ± 10%	65	66	7.9	9.1
Tafel slope/mV dec^{-1} ± 5%	81	84	66	81

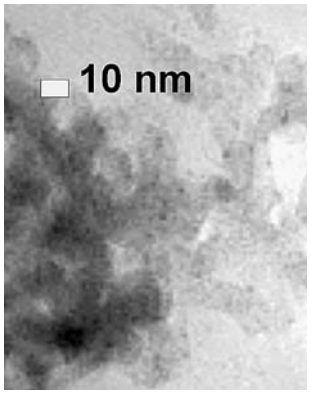

Fig. 5. TEM picture showing platinum nanoparticles (black) deposited on oxidized carbon aerogel (grey) oxCA#2.

Comparison of CA#1 and CA#2 electrochemical data in Table 2 confirms that the structural difference of the two carbons did not induce any measurable difference in either platinum activity or active surface area. Interestingly, the larger number of micropores in CA#1 than in CA#2 which could have been a drawback [27] (trapping of platinum particles) did not induce a measurable decrease in performance. Nevertheless, although the active platinum surface areas are satisfactory, they are about 40 % inferior to the geometrical surface areas that can be calculated from the Pt-particle diameters (d) observed on the TEM pictures with the well-known formula $6/\rho \cdot d$, ρ being the platinum bulk density.

This may be due to the relatively high platinum surface loadings (40–80 $\mu g\ cm^{-2}$) used on the EDT yielding possible disconnection of some platinum particles. It could also simply result from the ''hidden'' part of the platinum that contacts the carbon surface [25] which becomes greater as particle size decreases. The similarity of the platinum deposit kinetic activity on CA#1 and CA#2 further means that it will be possible in future work to make new catalytic layers based on Pt-doped carbon aerogels with different structures but identical platinum deposit in terms of surface area and intrinsic activity. This should be beneficial in studying the structural improvements (pore-size distribution optimization) of new PEMFC catalytic layers based on carbon aerogels. Indeed, the platinum deposit properties being independent of the carbon aerogel porous structure, the differences in cell performance will be principally governed by the structure of the catalytic layer.

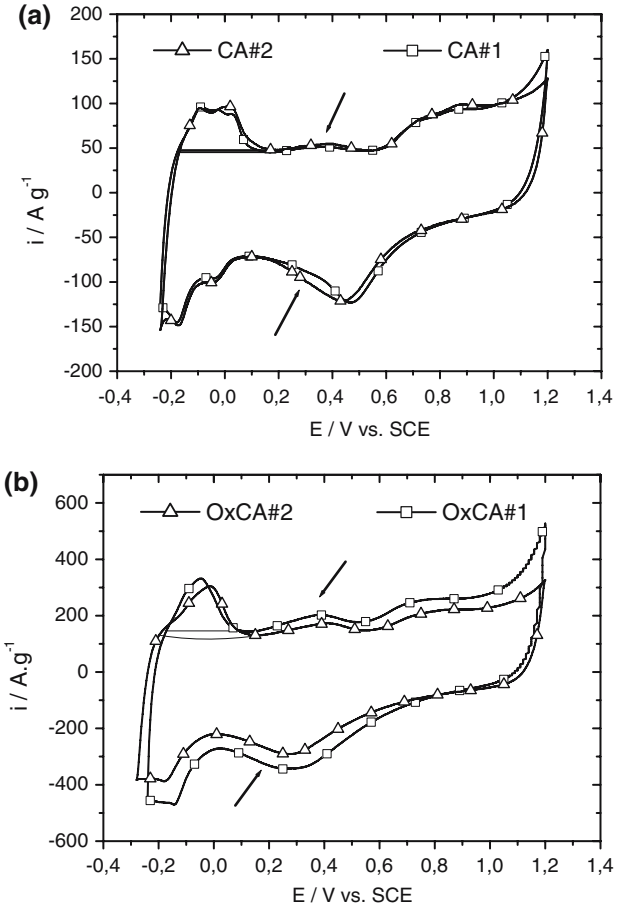

Fig. 6. Voltammograms recorded at 0.1 V s^{-1} in 1 M H_2SO_4 at 20 °C on 0.196 cm^2 glassy carbon disk electrode for Pt surface area determination on (a) raw carbon aerogels CA#1 & 2 (85 ± 4$\mu g_{Pt}\ cm^{-2}$) and (b) oxidized carbon aerogels oxCA#1 & 2 (40 ± 2$\mu g_{Pt}\ cm^{-2}$).

Looking further at Table 2, it appears that the specific activity of platinum on oxCA is much lower than platinum on raw CA. The specific ORR activity (A $cm^{-2}{}_{Pt}$) of Pt/oxCA samples is 7 times lower than that of Pt/CA samples. There may be at least two reasons for this: (1) the size of platinum particles is too small on Pt/oxCA samples and the nanoparticle size effect is detrimental [28, 29] (2) the platinum particles, due to their smallness, are located more deeply in the porous network of the carbon aerogel which implies a more difficult access to oxygen and thus a decrease in the ORR performance. By taking into account the diffusion of oxygen (homogeneous flooded model) in layers comprising Pt-doped carbon black and Nafion deposited on the RDE, Antoine et al. [30] showed that the oxygen diffusion limitation was not significant as long as the absolute overpotential was lower than 0.45 V vs NHE. Therefore, since our ORR activity measurements were carried out at 0.39 V vs NHE, it is more probable that the low activity of the Pt/oxCA catalysts is mainly due to the platinum particle-size effect. It could also be argued that the surface oxides are detrimental to the ORR but there is no known result which supports this hypothesis. In addition, the presence of oxides should be an advantage rather than a drawback because it increases the wetability of the carbon and thus promote access of the electrolyte to the platinum deposited on the carbon surface.

4. Conclusion

Two low bulk-density carbon aerogels with high porous volumes and surface areas, essentially differentiated by their pore-size distributions, were compared as

substrates for platinum deposition. The pore-sizes which contributed predominantly to the large porous volume of the two carbon aerogels were in the 50–66 nm range for CA#1 and in the 30–38 nm range for CA#2. Two different Pt-insertion techniques based on carbon aerogel aqueous impregnation were used. The structural difference between the two carbon aerogels was shown to yield no measurable difference in platinum deposit properties (i.e. active surface area, ORR activity).

The electrochemical results showed that carbon aerogel supported platinum are very promising catalysts for future performance improvements of PEMFC catalytic layers. The PEMFC cathode may especially benefit from the high porosity and large nanopore-size of the carbon aerogels.

The platinum insertion technique on raw carbon aerogels (anionic technique) gave the best results in terms of specific activity with almost 30 A g^{-1} at 20 °C in 1 M H_2SO_4 at 0.841 V/NHE in RDE experiments with 85 ± 4 μg cm^{-2} Pt loading. The insertion technique on oxidized carbon aerogels showed that very high platinum dispersion can be obtained (active Pt surface area up to 125 m^2 g^{-1}) but the activity of these catalysts is low, probably because of the particle size effect which is detrimental for small (~1 nm) platinum particles. Increasing the size of the platinum particles on these materials will be an interesting way of improving this result.

Acknowledgement

The authors acknowledge Mr Perrin of CEMEF, Sophia-Antipolis, for the TEM analysis.

References

1. P. Costamagna and S. Srinivasan, *J. Power Sources* **102** (2001) 242.
2. N. Hotz, M.-T. Lee, C.P. Grigoropoulos, S.M. Senn and D. Poulikakos, *Int. J. Heat Mass Tran.* **49** (2006) 2397.
3. C. Stone and A.E. Morrison, *Solid State Ionics* **152–153** (2002) 1.
4. W.G. Colella, M.Z. Jacobson and D.M. Golden, *J. Power Sources* **150** (2005) 150.
5. M. Granovskii, I. Dincer and M.A. Rosen, *Int. J. Hydrogen Energy* **31** (2006) 337.
6. C. Jaffray and G.A. Hards, Precious metal supply requirements, *in* W. Vielstich, A. Lamm and H.A. Gasteiger (Eds), 'Handbook of Fuel Cells – Fundamentals, Technology and Applications', Vol. 3 (Wiley, Chichester, 2003), pp.509–513.
7. H.A. Gasteiger, S.S. Kocha and F.T. Wagner, *App. Cat. B* **56** (2005) 9.
8. A.L. Dicks, *J. Power Sources* **156** (2006) 128.
9. A.W.P. Fung, G.A.M. Reynolds, Z.H. Wang, M.S. Dresselhaus, G. Dresselhaus and R.W. Pekala, *J. Non-Cryst. Solids* **186** (1995) 200.
10. M. Uchida, Y. Aoyama, N. Eda and A. Ohta, *J. Electrochem. Soc.* **142** (1995) 4143.
11. A. Smirnova, X. Dong, H. Hara, A. Vasiliev and N. Sammes, *Int. Hydrogen Energy* **30** (2005) 149.
12. D.A. Stevens and J.R. Dahn, *J. Electrochem. Soc.* **150** (2003) A770.
13. Z. Hou, B. Yi and H. Zhang, *Electrochem. Solid-State Lett.* **6** (2003) A232.
14. R.W. Pekala, *J. Mater. Sci.* **24** (1989) 3221.
15. K. Yasuda and Y. Nishimura, *Mat. Chem. Phys.* **82** (2003) 921.
16. H. Hao, L. Quach, J. Korah, W.A. Spieker and J.R. Regalbuto, *J. Mol. Cat. A* **219** (2004) 97.
17. S. Brunauer, P.H. Emmet and E. Teller, *J. Amer. Chem. Soc.* **60** (1938) 309.
18. M.M. Dubinin, *Adv. Colloid Interface Sci.* **2** (1968) 217.
19. J.C.P. Broekhoff and J.H. de Boer, *J. Catal.* **9** (1967) 8.
20. N. Job, A. Théry, R. Pirard, J. Marien, L. Kocon, J.-N. Rouzaud, F. Béguin and J.-P. Pirard, *Carbon* **43** (2004) 2481.
21. A.J. Bard and L.R. Faulkner, *Electrochemical Methods: Fundamentals and Applications* (Wiley, New York, 1992), pp. 283.
22. K.S.W. Sing, D.H. Everett, R.A.W. Haul, L. Moscou, R.A. Pierotti, J. Rouquérol and T. Siemienniewska, *Pure Appl. Chem.* **57** (1985) 603.
23. G.W. Scherer, *J. Non-Cryst. Solids* **225** (1998) 192.
24. I. Bautista-Toledo, J. Rivera-Utrilla, M.A. Ferro-Garcia and C. Moreno-Castilla, *Carbon* **32** (1994) 93.
25. J. Marie, S. Berthon-Fabry, P. Achard, M. Chatenet, A. Pradourat and E. Chainet, *J. Non-Cryst. Solids* **350** (2004) 88.
26. K. Kinoshita, *Carbon : Electrochemical and Physicochemical Properties* (John Wiley & Sons, New-York, 1988), pp. 309.
27. Z. Hou, B. Yi and H. Zhang, *Electrochemical and Solid-State Letters* **6** (2003) A232.
28. S. Mukerjee, *J. App. Electrochem.* **20** (1990) 537.
29. Y. Takasu, N. Ohashi, X.-G. Zhang, Y. Murakami, H. Minagawa, S. Sato and K. Yahikozawa, *Electrochim. Acta* **41** (1996) 2595.
30. O. Antoine, Y. Bultel and R. Durand, *J. Electroanal. Chem.* **499** (2001) 85.